Nanoscale

Cite this: *Nanoscale*, 2011, **3**, 2950

www.rsc.org/nanoscale

PAPER

Site-specific immobilization of gold binding polypeptide on gold nanoparticle-coated graphene sheet for biosensor application†

MinHo Yang,[a] Bong Gill Choi,[a] Tae Jung Park,*[b] Nam Su Heo,[b] Won Hi Hong[a] and Sang Yup Lee*[ab]

Received 22nd February 2011, Accepted 31st March 2011
DOI: 10.1039/c1nr10197h

The effective and strong immobilization of enzymes on solid surfaces is required for current biological applications, such as microchips, biofuel cells, and biosensors. Gold-binding polypeptide (GBP), a genetically designed peptide, possesses unique and specific interactions with a gold surface, resulting in improved enzyme stability and activity. Herein we demonstrated an immobilization method for biosensor applications through site-specific interactions between GBP-fused organophosphorus hydrolase (GBP-OPH) and gold nanoparticle-coated chemically modified graphene (Au-CMG), showing enhanced sensing capability. A flow injection biosensor was fabricated by using GBP-OPH/Au-CMG to detect paraoxons, a model pesticide, showing higher sensitivity, lower detection limit and better operating stability compared that of OPH/Au-CMG. This strategy, which integrates biotic and abiotic moieties through site-specific interactions, has a great potential for use in biosensing and bioconversion process.

Introduction

There is a great interest in the creation of enzyme-based nanoobjects that can provide bioelectrocatalytic interfaces with multifunctionality for numerous applications, such as biocatalysis, biosensors, biofuel cells, and bioelectronic devices.[1] In particular, an efficient biosensor can be developed by employing the biocatalytic capability of an enzyme combined with transducer materials, such as carbon allotropes and metal nanoparticles (NPs), which can produce a signal proportional to the amount of target analyte.[2] A key to the practical implementation of both components for biosensors is the robust immobilization of enzymes while preserving the activity and stability of the enzymes on the surface of transducer. To this end, much effort has been exerted to develop strategies for immobilizing enzymes stably and functionally onto the substrates; various methods including physical and/or chemical attachment, entrapment, and cross-linking have been employed.[3] However, problems still exist in minimizing the inconsistency and loss of enzyme activity (or even enzyme denaturation) because of random orientation, uncontrolled conformation, and different loading of enzymes. Here, we report the development of a strategy for the site-specific immobilization of gold-binding polypeptide (GBP)-fused enzymes onto gold (Au) NP-anchored graphene sheets and its use for the fabrication of electrochemical biosensors. Using organophosphorus hydrolase (OPH) as a model enzyme, we demonstrate that this electrochemical biosensor system can detect pesticides with a fast response time, low detection limit, and high sensitivity.

Genetically designed polypeptides (GDPs) have been attracting much attention as molecular and nanoscale building blocks in nanotechnology due to their specificity, selectivity and versatility in the interaction with various solid surfaces and other molecules.[4] In particular, fusion proteins with dual-functionality have been widely used to achieve effective and selective immobilization of biomolecules onto the specific solid surface, while providing the ability to interact with other molecules, including biomolecules.[5] The major advantages of the immobilization of these fusion enzymes on biosensors are the preservation of natural structures, high catalytic activities, and the conditions for specific immobilization.[6] For instance, GBP has been employed as a fusion partner in sensing elements by surface plasmon resonance.[7–9] Also, the morphologies and the activities of enzymes could be controlled through specific immobilization of genetically fused enzymes.[10] Although GDPs allow facile, simple and robust immobilization for biomolecules, there have been few reports on their use in electrochemical biosensors.[11]

Recently, chemically modified graphenes (CMGs) have attracted much attention as candidates for diverse applications in electronics, sensors, and energy storage/conversion, due to their extraordinary properties as well as the possibility of their large-scale production based on wet chemistry.[12] CMGs can serve as

[a]*Department of Chemical & Biomolecular Engineering (BK21 program), KAIST, 291 Daehak-ro, Yuseong-gu, Daejeon, 305-701, Republic of Korea. E-mail: leesy@kaist.ac.kr*
[b]*BioProcess Engineering Research Center, KAIST and Center for Nanobio Integration & Convergence Engineering, National Nanofab Center, 291 Daehak-ro, Yuseong-gu, Daejeon, 305-806, Republic of Korea. E-mail: tjpark@kaist.ac.kr*

† Electronic supplementary information (ESI) available: Additional data for characterization of GO, CMG, Au-CMG hybrids and comparison results of biosensing performance with other platforms (Table S1). See DOI: 10.1039/c1nr10197h

an ideal two-dimensional nanostructure of substrates for the deposition of inorganic nanomaterials because of the large surface area and outstanding electrical and mechanical properties. Coupling of CMGs and NPs further provides an effective strategy to develop multifunctional materials, offering catalytic, magnetic, sensing and optoelectronic materials.[13] Of particular interest is the decoration of Au NPs onto graphene sheets to fabricate a highly efficient biosensor with many advantages, including low resistance ohmic contacts, large accessible area and electrocatalytic effects.[14] For instance, Shan *et al.* demonstrated that introduction of Au NPs on graphene sheets increased the electroactive area and facilitated electron transfer, allowing efficient glucose detection.[15]

In this paper, we report the development of a general strategy for immobilization of OPH onto the conductive Au-CMG hybrid through strong site-specific interactions between the GBP-fused enzymes and the Au NPs anchored on CMGs. OPH was used as a model enzyme for its well-defined biocatalytic activity of degrading organophosphate (OP) compounds often used as pesticides and chemical warfare agents. The Au-CMG hybrid immobilized with GBP-OPH fusion protein was examined for rapid electron transfer, low charge transfer resistance, and high biocatalytic activity in flow-injection electrochemical biosensor.

Experimental

Preparation and synthesis of Au-CMG hybrid

Graphene oxides (GOs) were prepared from graphite powder (Sigma-Aldrich, <20 μm) *via* the modified Hummer.[16] Prior to synthesis of the Au-CMG nanohybrids, the dried graphite oxides (5 mg) were dispersed in deionized (DI) water (10 mL) by using an ultrasonic system (Fisher Scientific Model 500 ultrasonic, 350 W) for 30 min to obtain the fully exfoliated GOs. Aqueous solution of exfoliated GOs (0.5 mg mL^{-1}, 2 mL) was mixed with an ethanolic solution of $HAuCl_4 \cdot 3H_2O$ (2×10^{-2} mmol, 2 mL) were mixed together and sonicated in bath-type sonicator (Branson 3510) for 5 min to obtain Au–GO nanohybrids. After dialysis was carried out to remove unreacted Au precursor, Au–GO nanohybrids were reduced by addition of hydrazine (10 μL) at 85 °C. The resulting mixture was purified by filtration and dialysis for one week to remove remaining hydrazine, and dried overnight under vacuums at 60 °C.

Preparation of GBP-OPH fusion protein

OPH was used as a model protein for the immobilization onto the RGO-Au electrode and the hydrolysis of the OP substrate. Six histidine (6His) residues were introduced to facilitate purification of fusion proteins by metal affinity chromatography. The DNA fragment encoding incomplete 6His-GBP was first obtained by polymerase chain reaction (PCR) amplification using the primers P1 (5′-GAAACAGCATATGCACCATCACCATCACCACCACGGCAAAACCCAGGCGACCAG-3′) and P2 (5′-GGAATTCAGACTGAATGGTACCGCTCGTCGCTTGGGTTTTACCGTGCATAGATT-3′), and the plasmid pTGE as a template.[8] For the cloning of mature OPH (mOPH) gene, PCR amplification was carried out using the primers P3(5′-GAAATTCCATATGCATCATCACCACCACCACGGATCGATCGGCACAGGCGA-3′) and P4 (5′-AAAACTCGAGTGACGCCCGCAAGGTCGGTGA-3′), and the genomic DNA of *Flavobacterium* sp. ATCC27551 as a template. The PCR product of the 6His-GBP was digested with *Nde*I and *Eco*RI, and the PCR product of the mOPH gene was digested with *Eco*RI and *Xho*I, and then ligated into the same sites of pET-22b(+) to construct pET-6HGBP-mOPH. For the production of 6His-GBP-OPH fusion protein, *Escherichia coli* BL21(DE3) (F-*ompT hsdS*$_B$ (r_B^- m_B^-) *gal dcm* (DE3)) harboring pET-6HGBP-mOPH was cultivated in 100 mL Luria-Bertani medium supplemented with ampicillin (100 μg mL^{-1}) in a shaker (37 °C, 200 rpm). After the addition of isopropyl-β-D-thiogalactopyranoside for protein expression, cells were further cultivated for 6 h and disrupted by sonication for 1 min at 20% output. After centrifugation (16 000 *g*, 10 min, 4 °C), the insoluble pellet fraction was stored for the protein purification.

Immobilization of GBP-OPH on Au-CMG hybrid

The immobilization of GBP-OPH on Au-CMG hybrids was carried out in phosphate-buffered saline (PBS, pH 7.4) solution at room temperature. In brief, 200 μL of GBP-OPH solution was added into 2 mL Au-CMG hybrid solution and allowed to the self assembly for ~30 min through the site-specific affinity of GBP with Au NPs. In addition, the control OPH/Au-CMG was prepared by a same protocol of GBP-OPH/Au-CMG.

Characterization

Transmission electron microscopy (TEM) measurements were carried out with a JEM-2100F high-resolution TEM (HR-TEM) at acceleration voltage of 200 kV. The scanning electron microscopy (SEM) images were obtained using a field emission SEM (FEI Sirion model) equipped with a Schottky emitter in high stability. The atomic forced microscopy (AFM) images were recorded on XE-100 instruments (Park Systems) in the non-contact mode with silicon probes at scanning rate of 1 Hz. The X-ray diffraction (XRD) data were obtained on a Rigaku D/max IIIC (3 kW) with a q/q goniometer equipped with a Cu-Kα radiation generator. The diffraction angle of the diffractograms was in the range of $2\theta = 2°$–$90°$. The X-ray photon spectroscopy (XPS) data were obtained using a VG multilab 2000 (Thermo VG Scientific) with a monochromatic Mg-Kα X-ray source ($h\nu = 1253.6$ eV) under 10^{-7} Torr vacuum analysis chamber. The high resolution scans of C and low resolution survey scans were analyzed for each sample at least two separated locations. All circular dichroism (CD) spectra were taken using a Jasco J-815 spectropolarimeter fitted with a 150 W xenon lamp, scan speed of 50 nm min^{-1}, and response time of 5 s. Quartz cells of 0.5 mm optical path length were used. Thermogravimetric analysis (TGA) was performed on a TGA N1000 (Shinco) using a heating rate of 10 °C min^{-1}. Cyclic voltammetry (CV) and AC impedance were analyzed by a CHI 760D electrochemical workstation (CH Instruments) with a conventional three-electrode electrochemical cell using a glassy carbon working electrode, an Ag/AgCl (3 M KCl) reference electrode, and a platinum wire counter electrode. All potentials were recorded with respect to the reference electrode. AC impedance was carried out in range from 0.01 Hz to 100 kHz at constant 10 mV amplitude. A homemade flow cell with the interdigitated electrodes was connected to syringe pump

for flow injection anlaysis (FIA). The amperometric responses were then performed with FIA systems in N_2-saturated PBS solution at a polarization potential of 0.85 V and at a flow rate of 1 mL min^{-1} from the hydrodynamic voltammetric data.

Results and discussion

Scheme 1 illustrates the site-specific immobilization strategy for development of a GBP-OPH/Au-CMG hybrid and subsequently for fabrication of a flow-injection electrochemical biosensor to detect OPs. The stable and oriented immobilization of enzymes on the solid surface in electrochemical biosensors is of prime importance in order to effectively transducer biological activities to electrical signals. The GBP-OPH fusion protein used in this study was constructed by genetic engineering strategies and produced in recombinant *E. coli.* The Au-CMG hybrids were prepared as transducer materials that can convert detection of target analytes into the electrical signal and amplify the signal. Prior to the preparation of hybrids, the exfoliated GO prepared based on Hummer method[16] was dispersed in DI water/ethanol bisolvent through sonication. The quality of GO was confirmed by AFM and TEM analysis (Fig. S1 and S2 in ESI†). After adding Au precursor ($HAuCl_4 \cdot 3H_2O$), the mixture was treated with sonication for 5 min at room temperature. GO has abundant oxygen-containing groups such as carboxylic groups at the edges and hydroxyl and epoxy groups on the basal plane.[17] These oxygenated defects on GO readily provide nucleation sites for the growth of Au NPs in bisolvent by sonication.[18] The prepared Au-GO sheets were reduced by the addition of hydrazine and incubated at 85 °C to obtain the Au-CMG hybrids, as verified by XPS data (Fig. S3 and S4 in ESI†).

Finally, 200 μg of GBP-OPH fusion protein was added for its immobilization onto the Au-CMG hybrids by site-specific interaction between the GBP and Au NPs. These hybrids were transferred to the interdigitated Au electrode, and then the electrodes were covered with plastic cover on holes for inlet, outlet, and two reference and counter electrodes. The resulting flow-injection biosensor device was used for the electrochemical detection of OP compounds.

Graphene is an ideal supporting material for making Au-CMG hybrid due to its two-dimensional nanostructure with large surface area and excellent electrical and mechanical properties.[12] AFM and TEM images show the uniform decoration of Au NPs on the surface of CMG as shown in Fig. 1. To examine the morphology of Au-CMG hybrid, the samples were dropped on the cleaved mica surface and examined by AFM imaging. Au NPs were deposited on the CMG surface with the mean thickness of 10.03 nm (Fig. 1a). In addition, TEM images show that Au NPs were uniformly distributed on CMG sheets without aggregation (Fig. 1b and c). These results were consistent with that observed by energy dispersive X-ray spectroscopy (EDS) mapping (Fig. S5 in ESI†), showing that the average size of Au NPs was 8.1 ± 0.67 nm. The lattices in HR-TEM images have an interfringe distance of 2.35 Å, corresponding to (111) plane of Au NPs (Fig. 1d). The molecular binding of GBP onto the Au surface has been known to occur by the interaction with Au (111) plane structure through conformational recognition and internal stabilization.[19]

The percentage of Au NPs decorated on the surface of CMG was determined to be about 13.8 wt% by TGA of GO and Au-CMG hybrids (Fig. S6 in ESI†). In the case of GO, the TGA trace shows the first weight loss at around 100 °C due to the removal of physisorbed water. Two other significant drops in

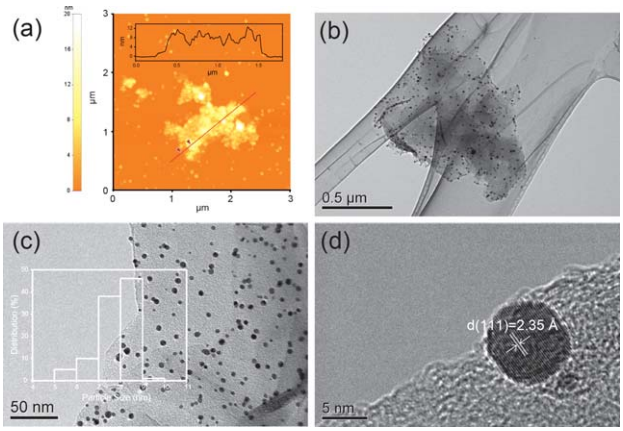

Fig. 1 (a) Tapping-mode AFM images of Au-CMG hybrids. The inset represents the line scan of that sample. (b–c) TEM images of the Au-CMG hybrids at different magnifications. The inset shown in panel (c) represents the size distribution plot of Au NPs in Au-CMG hybrids. (d) HR-TEM images of Au-CMG hybrids.

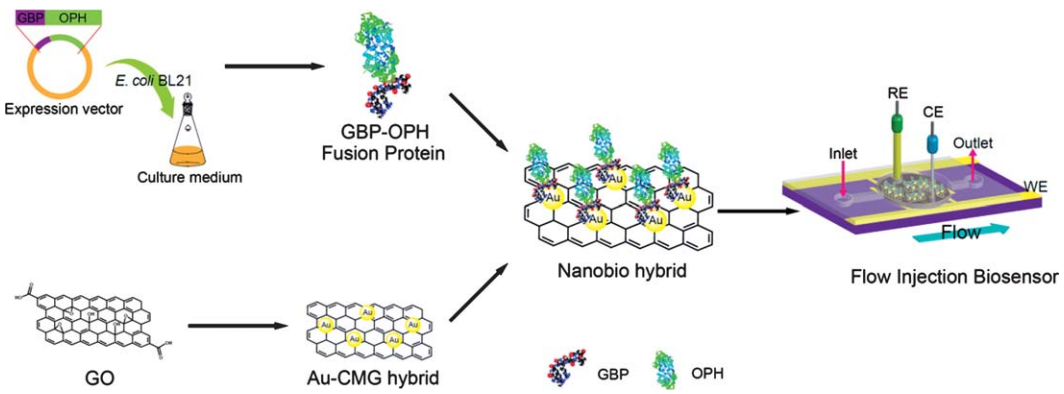

Scheme 1 Schematic diagram of fabrication of a GPB-OPH/Au-CMG flow injection biosensor (RE: reference electrode, CE: counter electrode, WE: working electrode).

weight take place at around 220 °C and 570 °C due to the pyrolysis of oxygen-containing groups on the surface of GO sheets, yielding CO, CO_2, and steam.[20] Compared with GO, Au-CMG shows higher thermal stability, indicating the successful removal of oxygen-containing groups by chemical reduction.[21] The Au (111) plane of Au-CMG hybrids was also characterized by the XRD (Fig. S7 in ESI†), whose profile exhibited several peaks from the Au NPs with a dominant diffraction peak at 38.1° for Au (111).[22] In addition, the broad graphite reflection was observed at 24.2°, indicating that Au-CMG hybrids were comprised of few layers.[23] Thus, the CMG sheets served as the well-defined mat for the assembly of Au NPs with uniform size distribution, and consequently provided binding sites for GBP-OPH fusion proteins.

To investigate molecular binding of GBP onto the Au surface, the Au 4f XPS spectra were analyzed before and after the immobilization of GBP-OPH on Au-CMG hybrids. As shown in Fig. 2a, the doublet peaks at 84.11 and 87.81 eV corresponding to Au^0 $4f_{7/2}$ and Au^0 $4f_{5/2}$, respectively, were observed. After immobilization of GBP-OPH on Au-CMG hybrids, the peak positions of Au^0 $4f_{7/2}$ and Au^0 $4f_{5/2}$ shifted to lower binding energies with decreased intensities, indicating the disorder or heterogeneity in the binding sites of Au NPs due to the highly attractive interface interactions of GBPs with the Au (111) planes

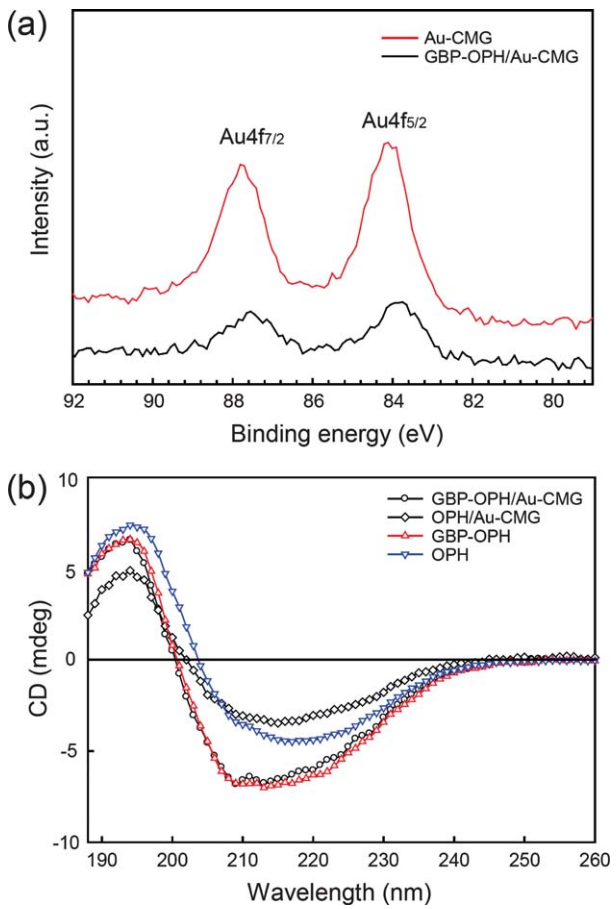

Fig. 2 (a) XPS spectra of Au-CMG (black line) and GBP-OPH/Au-CMG (red line). (b) CD spectra of OPH (blue inverted triangle), GBP-OPH (red open triangle), GBP-OPH/Au-CMG (black open circle) and OPH/Au-CMG (blue open diamond).

of Au-CMG hybrids. The conformational changes of GBP-OPH and OPH after immobilization onto Au-CMG hybrids were studied by CD spectroscopy as shown in Fig. 2b. The CD spectroscopy has been widely used to monitor the folding, stability, and conformational changes of proteins in solution or immobilized onto the colloidal surface, which arise from π–π* and n–π* transitions.[24] The secondary structure of GBP-OPH after immobilization onto the surface of Au-CMG hybrids was quite similar to that of free GBP-OPH, indicating no conformational changes of GBP-OPH during immobilization. However, the slight shift in negative peaks from 212 and 220 nm to 209 and 217 nm with a decrease in intensity revealed after immobilization of OPH onto the Au-CMG hybrid. This result indicates that the secondary structure of OPH was altered upon its immobilization on the surface of hybrids without GBP. Thus, the use of GBP-fusion approach for the immobilization of OPH on the Au NPs allows preservation of the native structure.

The electrochemical properties using the interdigitated Au electrodes modified by GBP-OPH/Au-CMG were examined. The surface of GBP-OPH/Au-CMG deposited onto the electrode was characterized by SEM as shown in ESI† (Fig. S8). The specific binding interactions between GBP-OPH fusion proteins and Au-CMG hybrids resulted in good immobilization of enzymes without aggregation. In order to verify the electron transfer of GBP-OPH/Au-CMG at the bioactive interface, CV analysis was performed in an electrolyte solution of $Fe(CN)_6^{3-/4-}$. It is well known that $Fe(CN)_6^{3-/4-}$ exhibits a surface-dependent behavior on the carbon electrode, which allows the characterization of the nature of the electrode surface and the kinetics of catalytic reaction.[25] Fig. 3a shows the typical CVs of Au-CMG hybrid with peak-to-peak separation (ΔE_p) of 64 mV, which is related to the electron transfer rate. The ideal electron transfer rate is 59 mV for one electron transferred on the electrode.[26] In general, the peak current (I_p) decreases and the ΔE_p increases after enzyme immobilization due to the blocking of the electron transfer. The GBP-OPH/Au-CMG showed a higher value of I_p and a smaller value of ΔE_p than those of OPH/Au-CMG. Furthermore, there is a well-defined linear relationship between I_p and square root of scan rate ($\nu^{1/2}$) for the GBP-OPH/Au-CMG, which means that the reaction is quasi-reversible and controlled by diffusion (Fig. S9 in ESI†). The electroactive surface area (A) for nanobio-hybrids was obtained by Randle-Ševčík equation,[26] which assumes mass transport only by diffusion.

$$I_p = 2.69 \times 10^5 n^{2/3} A D^{1/2} \nu^{1/2} C^* \quad (1)$$

The electroactive area for the GBP-OPH/Au-CMG was 0.289 cm^2 and that for OPH/Au-CMG was 0.205 cm^2. Thus, the electroactive fraction of GBP-OPH/Au-CMG was 94.5% and that of OPH/Au-CMG was 67.1%, which indicated that GBP-OPH was more stable and retained higher bioactivity on Au-CMG hybrids. The surface coverage (T^*) of GBP-OPH and OPH on the Au-CMG hybrids estimated to be 1.85×10^{-9} mol cm^{-2} and 1.32×10^{-9} mol cm^{-2}, respectively.[26] In both cases, an electroactive monolayer of enzymes on the surface of Au-CMG hybrids was formed. These results suggest that the self-associative behavior of GBP allows efficient immobilization of bioactive OPH on Au-CMG hybrids and enhanced accessibility of electroactive species, yielding excellent electrochemical properties.

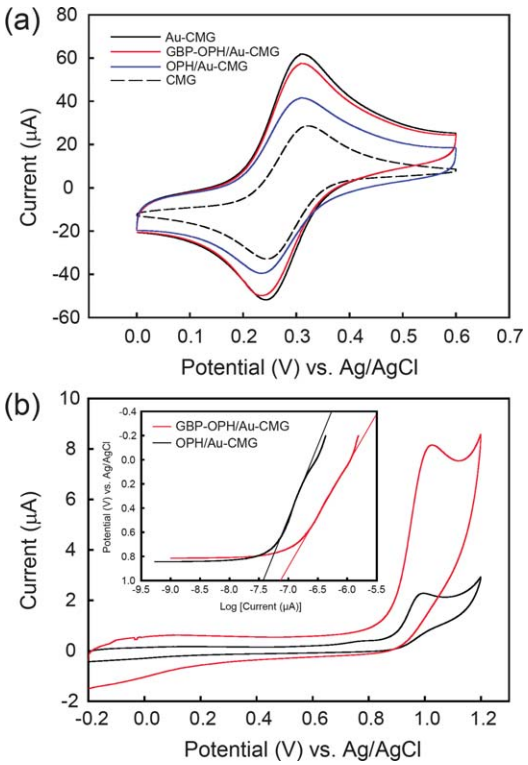

Fig. 3 (a) CVs of the CMG (dashed line), Au-CMG (black line), GBP-OPH/Au-CMG (red line), OPH/Au-CMG (blue line) in solution containing 5 mM $Fe(CN)_6^{3-/4-}$ and 0.1 M KCl at a scan rate of 50 mV s^{-1}. (b) CV on the GBP-OPH/Au-CMG (red line) and the OPH/Au-CMG (black line) in 1 mM paraoxon solution at a scan rate of 50 mV s^{-1}. The inset shows the Tafel plot obtained from CV.

The GBP-OPH/Au-CMG hybrid biosensor system was then examined for its capability to detect OP compounds by electrochemical analysis. As an example, paraoxon is chosen as a model OP chemical. Fig. 3b presents the CVs obtained with the GBP-OPH/Au-CMG and OPH/Au-CMG in a solution containing 1 mM paraoxon. The GBP-OPH/Au-CMG showed a substantially larger anodic signal and a lower onset point than the OPH/Au-CMG, likely resulting from a larger electroactive area and a higher electron transfer rate on the interface surface. In order to understand the possible reasons for facilitated electron transfer by employing the GBP-OPH fusion protein, the Tafel slope, related to the activation energy for electrochemical reactions, was estimated from the Butler-Volmer equation.[26]

$$\log i = \log i_0 + \frac{\alpha_A nF}{2.303RF}\eta \qquad (2)$$

The Tafel slope for GBP-OPH/Au-CMG (82.3 mV dec^{-1}) was smaller than that for OPH/Au-CMG (107.3 mV dec^{-1}), indicating that the GBP-OPH fusion protein requires a lower activation energy for the hydrolysis of paraoxon than OPH without GBP.

To understand the electron transport phenomena at the bioactive interfaces with GBP and without GBP, the Randle's equivalent circuit was chosen to fit the obtained impedance data. The Nyquist plot represents the reaction kinetics and diffusion behavior, and is related to the charge transfer resistance (R_{ct}) in series with Warburg impedance (Z_w).[26] As shown in Fig. 4a, the diameter of the semicircle corresponding to the value of R_{ct} for OPH/Au-CMG (70.39 Ω) was larger than that of GBP-OPH/Au-CMG (47.45 Ω) at a high frequency region. This indicates that the charge transfer became more efficient by using the GBP fusion protein, consistent with the CV results in Fig. 3a. At the low frequency region, the slope of the plot is linear due to the fractal geometry effects of the surface, suggesting a diffusion control system. According to the eqn (3),[27] the real (Z') or imaginary (Z'') part of the Warburg impedance is proportional to the reciprocal of the square root of the angular frequency ($\omega^{-1/2}$). Fig. 4b exhibits the plot of Z' *versus* $\omega^{-1/2}$, in which the slope at low frequency region provides the Warburg coefficients (σ) of both nanobio-hybrids. The σ values of GBP-OPH/Au-CMG were lower than those of OPH/Au-CMG. The diffusion coefficient (D) of electroactive molecules at the interfacial region was evaluated with eqn (4).[26]

$$Z_w = \sigma\omega^{-1/2}(1 - j) \qquad (3)$$

$$\sigma = \frac{RT}{n^2F^2A\sqrt{2}}\left(\frac{1}{D_O^{1/2}C_O^*} + \frac{1}{D_R^{1/2}C_R^*}\right) \qquad (4)$$

From the results shown in Fig. 4b, the hydrolyzed *p*-nitrophenol (PNP) at the GBP-OPH/Au-CMG interface diffused onto the

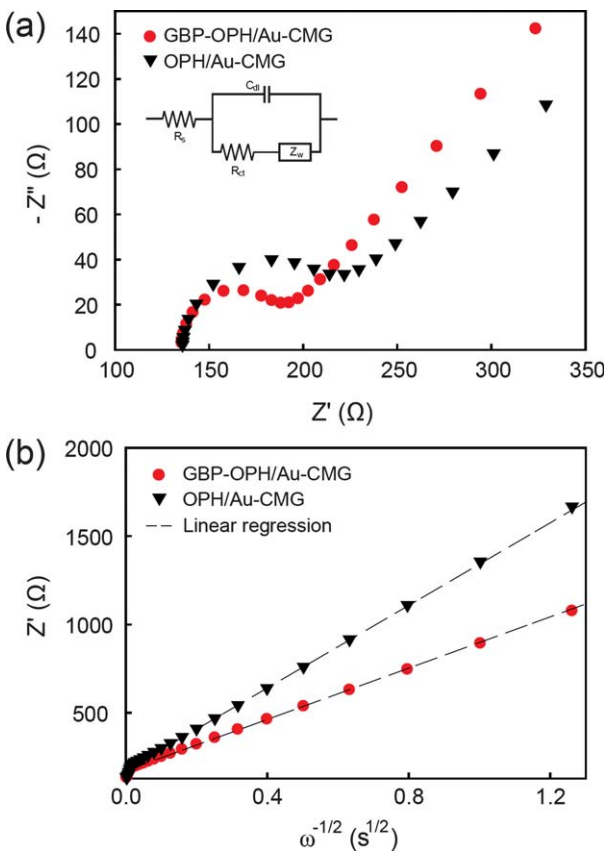

Fig. 4 (a) The Nyquist plot of GBP-OPH/Au-CMG (red circle) and OPH/Au-CMG (black inverted triangle) in 1 mM paraoxon solution. The inset is the equivalent circuit used for the analysis. (b) The plots of real part of impedance (Z') *versus* $\omega^{-1/2}$ obtained from the above solution at GBP-OPH/Au-CMG (red circle) and OPH/Au-CMG (black inverted triangle).

surface of Au-CMG hybrids was much faster compared with the OPH/Au-CMG interface. This seems to be due to that the self-associative behavior of GBP with Au NPs allowed construction of well-oriented structures at the interface of Au-CMG hybrid and enhances accessibility of PNP on the Au-CMG hybrid.

The degradation and detection mechanism of paraoxon by using GBP-OPH/Au-CMG are depicted in Scheme 2. The OPH triggers enzymatic hydrolysis of paraoxon coupled with releasing electroactive PNP, according to reaction 1.[28] The GBP-OPH/Au-CMG allowed not only retaining the enzyme activity without conformational change but also facilitating electron transfer of PNP. The successful construction of interface based on the hybrid system was based on two important factors. First, the GBP fusion protein provided binding specificity, enzyme stability, and well-oriented enzyme morphology, which resulted in high enzymatic activity and accessibility of chemicals to be detected. Second, CMG served as a good conductive support for facilitating electron transfer, preventing aggregation of Au NPs and large loading of Au NPs. Thus, the GBP-OPH/Au-CMG provides a synergistic platform for simultaneous functions of biocatalysis, electron transport and mass transfer, as confirmed by CV and impedance analyses.

To characterize the performance of the GBP-OPH/Au-CMG as an agrichemical biosensor, FIA with amperometric detection was performed. Fig. 5a shows the amperometric responses of GBP-OPH/Au-CMG and OPH/Au-CMG with increasing paraoxon concentrations (2 μM steps). At a polarization potential of 0.85 V, the anodic current increased temporally within 3 s and returned back to the buffer signal level. The resulting calibration plots showed a linear relationship in amperometric response. The sensitivities were 55.54 nA μM^{-1} for GBP-OPH/Au-CMG and 1.80 nA μM^{-1} for OPH/Au-CMG. The limits of detection (LOD, S/N = 3) were 9.54×10^{-8} and 4.67×10^{-7} M for GBP-OPH/Au-CMG and OPH/Au-CMG, respectively. As shown in Fig. 5b, the biosensor employing GBP-OPH showed a good operating stability compared with that using the native OPH; while the OPH/Au-CMG showed a gradual decrease of signal, a stable response was observed over the entire operation when using the

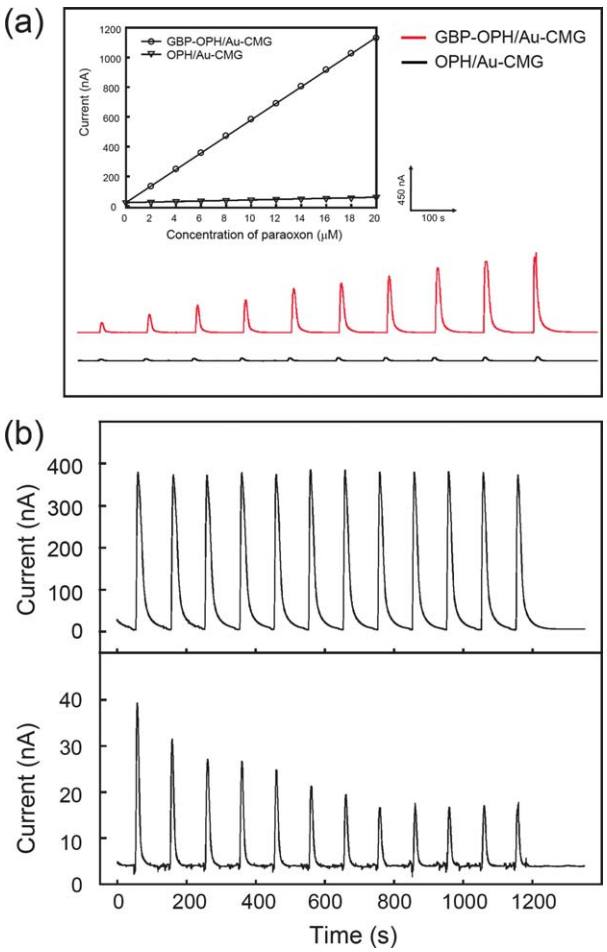

Fig. 5 (a) Amperometric responses to subsequent injection of 2 μM paraoxon to the flow cell transferred GBP-OPH/Au-CMG (red line) and OPH/Au-CMG (black line). The inset shows calibration curves of the current *versus* concentration of paraoxon. (b) The operating stability of GBP-OPH/Au-CMG (top) and OPH/Au-CMG (bottom), respectively. Conditions were follows; applied potential, +0.85 V; flow rate, 1 mL min^{-1}; paraoxon concentration, 6 μM.

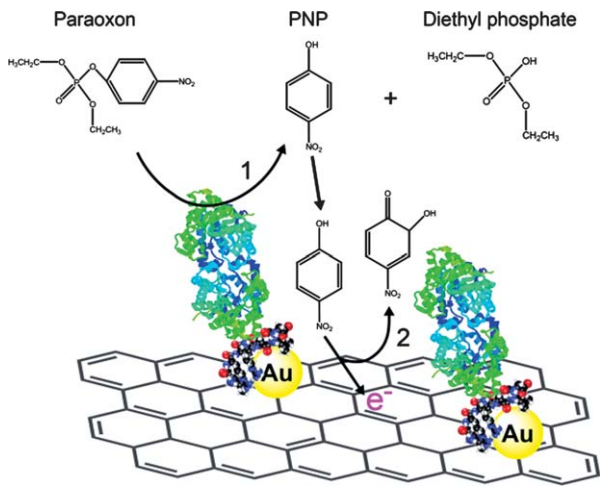

Scheme 2 Schematic representation of paraoxon hydrolysis by OPH (reaction 1) immobilized through GBP on the Au-CMG, and further oxidation of PNP (reaction 2).

GBP-OPH/Au-CMG. The detection performance of the GBP-OPH biosensor developed in this study is compared with those of other biosensors (see Table S1, ESI†). The GBP-OPH biosensor shows a higher sensitivity and a shorter response time for the paraoxon detection compared with other biosensors without using the GBP as a fusion partner.

Conclusions

In summary, we reported the development of an electrochemical biosensor system by stable and highly functional immobilization of GBP-fusion enzyme onto the Au-CMG, and its use for a rapid and sensitive electrochemical detection of an agrichemical. The high enzyme activity and rapid electrical communication of GBP-OPH/Au-CMG result from the well-oriented structure and unique properties of the system, such as large surface area and excellent catalytic and electrical properties. This GBP-OPH biosensor system was successfully applied for the detection of paraoxon as a model OP compound with a sensitivity of

55.54 nA μM^{-1}, LOD of 9.54×10^{-8} M, and response time of less than 3 s. Furthermore, the GBP-OPH/Au-CMG displayed a well-defined linear electrical response to the varying concentrations (2 to 20 μM) of paraoxon. Although we used OPH as a model enzyme and paraoxon as a target chemical to detect in this study, various applications can be realized by employing different enzymes to detect other chemicals using GBP as a fusion partner and Au-CMG as a conductive surface. It is expected that this hybrid electrochemical sensor system would be widely applicable in developing point-of-care devices for sensing chemicals.

Acknowledgements

This work was supported by the Technology Innovation Program (10037246) funded by the Ministry of Knowledge Economy (MKE, Korea).

Notes and references

1 (*a*) E. Katz and I. Willner, *Angew. Chem., Int. Ed.*, 2004, **43**, 6042–6108; (*b*) Y. Xiao, F. Patolsky, E. Katz, J. F. Hainfeld and I. Willner, *Science*, 2003, **299**, 1877–1881; (*c*) G. Piperberg, O. I. Wilner, O. Yehezkeli, R. Tel-Verred and I. Willner, *J. Am. Chem. Soc.*, 2009, **131**, 8724–8725; (*d*) F. Gao, L. Viry, M. Maugey, P. Poulin and N. Mano, *Nat. Commun.*, 2010, **1**, 1–7; (*e*) I. Baravik, R. Tel-Vered, O. Ovits and I. Willner, *Langmuir*, 2009, **25**, 13978–13983.
2 W. Yang, K. R. Ratinac, S. P. Ringer, P. Thordarson, J. J. Gooding and F. Braet, *Angew. Chem., Int. Ed.*, 2010, **49**, 2114–2138.
3 (*a*) H. R. Luckarift, J. C. Spain, R. R. Naik and M. O. Stone, *Nat. Biotechnol.*, 2004, **22**, 211–213; (*b*) U. T. Bronscheuer, *Angew. Chem., Int. Ed.*, 2003, **42**, 3336–3337; (*c*) R. A. Sheldon, *Adv. Synth. Catal.*, 2007, **349**, 1289–1307.
4 (*a*) M. Sarikaya, C. Tamerler, A. K.-Y. Jen, K. Schulten and R. Baneyx, *Nat. Mater.*, 2003, **2**, 577–585; (*b*) K. T. Nam, D.-W. Kim, P. J. Yoo, C.-Y. Chiang, N. Meethong, P. T. Hammond, Y.-M. Chiang and A. M. Belcher, *Science*, 2006, **312**, 885–888.
5 (*a*) T. Kacar, J. Ray, M. Gungrmus, E. E. Oren, C. Tamerler and M. Sarikaya, *Adv. Mater.*, 2009, **21**, 295–299; (*b*) C. Tamerler and M. Sarikaya, *ACS Nano*, 2009, **3**, 1606–1615.
6 R. D. Richins, A. Mulchandani and W. Chen, *Biotechnol. Bioeng.*, 2000, **69**, 591–596.
7 T. Kacar, M. T. Zin, C. So, B. Wilson, H. Ma, N. Gul-Karaguler, A. K.-Y. Jen, M. Sarikaya and C. Tamerler, *Biotechnol. Bioeng.*, 2009, **103**, 696–705.
8 T. J. Park, S. Y. Lee, S. J. Lee, J. P. Park, K. S. Yang, K.-B. Lee, S. Ko, J. B. Park, T. Kim, S. K. Kim, Y. B. Shin, B. H. Chung, S.-J. Ku, D. H. Kim and I. S. Choi, *Anal. Chem.*, 2006, **78**, 7197–7205.
9 (*a*) S. Ko, T. J. Park, H.-S. Kim, J.-H. Kim and Y.-J. Cho, *Biosens. Bioelectron.*, 2009, **24**, 2592–2597; (*b*) T. J. Park, M. S. Hyun, H. J. Lee, S. Y. Lee and S. Ko, *Talanta*, 2009, **79**, 295–301; (*c*) T. J. Park, S. Zheng, Y. J. Kang and S. Y. Lee, *FEMS Microbiol. Lett.*, 2009, **293**, 141–147; (*d*) S. Zheng, D.-K. Kim, T. J. Park, S. J. Lee and S. Y. Lee, *Talanta*, 2010, **82**, 803–809.
10 J. Wang, D. Bhattacharyya and L. G. Bachas, *Biomacromolecules*, 2001, **2**, 700–705.
11 (*a*) Z. Naal, J.-H. Park, S. Bernhard, J. P. Shapleigh, C. A. Batt and H. D. Abruña, *Anal. Chem.*, 2002, **74**, 140–148; (*b*) M. Campàs, B. Prieto-Simón and J.-L. Marty, *Semin. Cell Dev. Biol.*, 2009, **20**, 3–9.
12 (*a*) S. Park and R. S. Ruoff, *Nat. Nanotechnol.*, 2009, **4**, 217–224; (*b*) G. Eda and M. Chhowalla, *Adv. Mater.*, 2010, **22**, 2392–2415; (*c*) E. Yoo, J. Kim, E. Hosono, H. Zhou, T. Kudo and I. Honma, *Nano Lett.*, 2008, **8**, 2277–2282; (*d*) C. Shan, H. Yang, J. Song, D. Han, A. Ivsaka and L. Niu, *Anal. Chem.*, 2009, **81**, 2378–2382.
13 (*a*) Y. Si and E. T. Samulski, *Chem. Mater.*, 2008, **20**, 6792–6797; (*b*) J. Lu, I. Do, L. T. Drzal, R. M. Worden and I. Lee, *ACS Nano*, 2008, **2**, 1825–1832; (*c*) C. Xu and X. Wang, *Small*, 2009, **5**, 2212–2217; (*d*) S. Watcharotone, D. A. Dikin, S. Stankovich, R. Piner, I. Jung, G. H. B. Dommett, G. Evmenenko, S.-E. Wu, S.-F. Chen, C.-P. Liu, S. T. Nguyen and R. S. Ruoff, *Nano Lett.*, 2007, **7**, 1888–1892; (*e*) J. Shen, Y. Hu, M. Shi, N. Li, H. Ma and M. Ye, *J. Phys. Chem. C*, 2010, **114**, 1498–1503.
14 (*a*) K. Jasuja and V. Berry, *ACS Nano*, 2009, **3**, 2358–2366; (*b*) A. Benayad, H.-J. Shin, H. K. Park, S.-M. Yoon, K. K. Kim, M. H. Jin, H.-K. Jeong, J. C. Lee, J.-Y. Choi and Y. h. Lee, *Chem. Phys. Lett.*, 2009, **475**, 91–95; (*c*) F. Li, H. Yang, C. Shan, Q. Zhang, D. Han, A. Ivaska and L. Niu, *J. Mater. Chem.*, 2009, **19**, 4022–4025.
15 C. Shan, H. Yang, D. Han, Q. Zhang, A. Ivaska and L. Niu, *Biosens. Bioelectron.*, 2010, **25**, 1070–1074.
16 W. S. Hummers and R. E. Offeman, *J. Am. Chem. Soc.*, 1958, **80**, 1339.
17 G. Goncalves, P. A. A. P. Marques, C. M. Granadeiro, H. I. S. Nogueira, M. K. Singh and J. Grácio, *Chem. Mater.*, 2009, **21**, 4796–4802.
18 H. S. Park, B. G. Choi, S. H. Yang, W. H. Shin, J. K. Kang, D. Jung and W. H. Hong, *Small*, 2009, **5**, 1754–1760.
19 C. R. So, C. Tamerler and M. Sarikaya, *Angew. Chem., Int. Ed.*, 2009, **48**, 5174–5177.
20 A. Lerf, H. He, M. Forster and J. Klinowski, *J. Phys. Chem. B*, 1998, **102**, 4477–4482.
21 S. Stankovich, D. A. Dikin, R. D. Piner, K. A. Kohlhaas, A. Kleinhammes, Y. Jia, Y. Wu, S. T. Nguyen and R. S. Ruoff, *Carbon*, 2007, **45**, 1558–1565.
22 R. Cui, C. Liu, J. Shen, D. Gao, J.-J. Zhu and H.-Y. Chen, *Adv. Funct. Mater.*, 2008, **18**, 2197–2204.
23 K. S. Subrahmanyam, S. R. C. Vivekchand, A. Govindaraj and C. N. R. Rao, *J. Mater. Chem.*, 2008, **18**, 1517–1523.
24 G. D. Fasman, *Circular Dichroism and the Conformational Analysis of Biomolecules*, Plenum Press, New York, 1996.
25 R. L. McCreery, *Chem. Rev.*, 2008, **108**, 2646–2687.
26 A. J. Bar and L. R. Faulkner, *Electrochemical Methods: Fundamentals and Applications*, Wiley, New York, 2001.
27 R. P. Janek and W. R. Fawcett, *Langmuir*, 1998, **14**, 3011–3018.
28 S. Mulchandani, P. Mulchandani, W. Chen, J. Wang and L. Chen, *Anal. Chem.*, 1999, **71**, 2246–2249.

